Article

Single-Component Magnetic Conductors Based on MoS Trinuclear Clusters with Outer Dithiolate Ligands

Rosa Llusar, Santiago Uriel, Cristian Vicent, Juan M. Clemente-Juan, Eugenio Coronado, Carlos J. Gmez-Garca, Benoit Brada, and Enric Canadell

J. Am. Chem. Soc., **2004**, 126 (38), 12076-12083• DOI: 10.1021/ja0474244 • Publication Date (Web): 04 September 2004

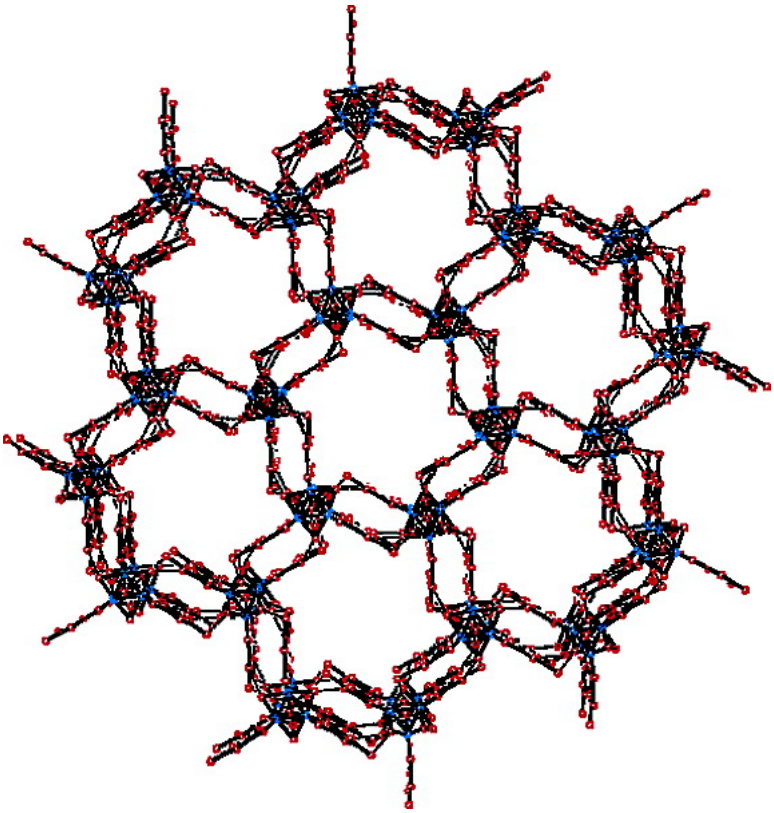

J|A|C|S
ARTICLES
Published on Web 09/04/2004

Single-Component Magnetic Conductors Based on Mo_3S_7 Trinuclear Clusters with Outer Dithiolate Ligands

Rosa Llusar,*,† Santiago Uriel,*,‡ Cristian Vicent,† Juan M. Clemente-Juan,§ Eugenio Coronado,§ Carlos J. Gómez-García,§ Benoit Braïda,# and Enric Canadell#

Contribution from the Departament de Ciències Experimentals, Universitat Jaume I, Campus de Riu Sec, Avda. Sos Baynat s/n, E-12080, Castelló, Spain, Departamento de Química Orgánica-Química Física, Centro Politécnico Superior, Universidad de Zaragoza-ICMA, María de Luna 3, E-50015, Zaragoza, Spain, Instituto de Ciencia Molecular, Universitat de Valencia, c/ Dr. Moliner no 50, E-46100, Spain, and Institut de Ciència de Materials de Barcelona (CSIC), Campus de la UAB, E-08193 Bellaterra, Spain

Received May 3, 2004; E-mail: llusar@exp.uji.es; suriel@unizar.es

Abstract: A trinuclear cluster complex containing the Mo_3S_7 central unit coordinated to dithiolate ligands, in particular the organic dmit (1,3-dithia-2-thione-4,5-dithiolate) anion, has been used to prepare a single-component molecular conductor formed by the threefold symmetry magnetic building block $Mo_3S_7(dmit)_3$ (**1**). The $[Mo_3S_7(dmit)_3]^{2-}$ ($[\mathbf{1}]^{2-}$) diamagnetic anion forms dimers by interaction between the electrophilic cluster axial sulfur atoms and the sulfur atoms of the outer dithiolate ligand. Additional contacts between adjacent dmit ligands result in chain formation. The two-electron oxidation of $[\mathbf{1}]^{2-}$ yields to a three-dimensional molecular solid formed by neutral $Mo_3S_7(dmit)_3$ (**1**) units with partially filled molecular orbitals, which exhibits sizable intermolecular electronic interactions together with a significant electron delocalization. It also contains large open channels. The interactions responsible for the conducting properties have been identified using a first-principle DFT approach and the calculated electronic structure has allowed us to model the magnetic behavior of the material with two competing antiferromagnetic interactions to produce a spin-frustrated extended network. The potential of this Mo_3S_7 cluster complex to be modified together with the capability of filling the open channels with doping species paves the way to an entirely new set of molecular conductors and/or magnets.

1. Introduction

The long date challenge of preparing a metallic solid built exclusively from molecular units was realized with the successful marriage of TCNQ (tetracyanoquinodimethane) and TTF (tetrathiafulvalene)[1,2] to form the charge-transfer salt $[TTF]^{\delta+}$-$[TCNQ]^{\delta-}$. This discovery launched an enormous interest in these molecular conductors as many exciting physical phenomena such as superconductivity, field induced spin density waves, magnetic oscillations, etc. were found in these low-dimensional systems.[3] A common feature of practically all molecular metals is that they are at least two-component systems. This is due to the fact that some kind of electron transfer is needed to lead to the partial emptying and/or filling of bands needed to create the metallic state. Theoretical work on the so-called 'two-band systems' challenged this notion by showing that the electron transfer could internally occur between two types of bands of the same component[4] and that metal bis(dithiolene) molecules could lead to single-component molecular metals.[5] This hypothesis has been recently confirmed by Kobayashi's group, almost thirty years after the TTF-TCNQ discovery, opening large expectations for a renewal of the field.[6]

Another relevant topic in this area is that of obtaining molecular materials mixing conductivity or superconductivity with other physical phenomena (magnetism in particular). Most of these materials are usually made by combining a conducting organic network with an inorganic magnetic component. Some relevant results in this area have been the discoveries of two series of paramagnetic superconductors; the first one is the monoclinic $(BEDT\text{-}TTF)_4[AM(C_2O_4)_3]$ solvent (BEDT-TTF = bis(ethylenedithio)tetrathiafulvalene; A = H_3O; M(III) = Cr, Fe,) series with the organic molecules packed in the β arrangement.[7,8] The second one consists of BEDT-TSeF (BEDT-TSeF = bis(ethylenedithio)tetraselenafulvalene) charge-transfer

† Universitat Jaume I.
‡ Universidad de Zaragoza-ICMA.
§ Universitat de Valencia.
# Institut de Ciència de Materials de Barcelona (CSIC).

(1) Ferraris, J.; Cowan, D. O.; Walatka, V.; Perlstein, J. H. *J. Am. Chem. Soc.* **1973**, *95*, 948−949.
(2) Coleman, L. B.; Cohen, M. J.; Sandman, D. J.; Yamagishi, F. G.; Garito, A. F.; Heeger, A. J. *Solid State Commun.* **1973**, *12*, 1125−1132.
(3) Ishiguro, T.; Yamaji, K.; Saito, G. *Organic Superconductors*, 2nd ed.; Springer-Verlag: Berlin, 1998.
(4) Canadell, E.; Rachidi, I. E. I.; Ravy, S.; Pouget, J. P.; Brossard, L.; Legros, J. P. *J. Phys. (France)* **1989**, *50*, 2967−2981.
(5) Canadell, E. *New J. Chem.* **1997**, *21*, 1147−1159.
(6) Tanaka, H.; Okano, Y.; Kobayashi, H.; Suzuki, W.; Kobayashi, A. *Science* **2001**, *291*, 285−287.
(7) Kurmoo, M.; Graham, A. W.; Day, P.; Coles, S. J.; Hursthouse, M. B.; Caulfield, J. L.; Singleton, J.; Pratt, F. L.; Hayes, W.; Ducasse, L.; Guionneau, P. *J. Am. Chem. Soc.* **1995**, *117*, 12209−12217.
(8) Rashid, S.; Turner, S. S.; Day, P.; Howard, J. A. K.; Guionneau, P.; McInnes, E. J. L.; Mabbs, F. E.; Clark, R. J. H.; Firth, S.; Biggs, T. *J. Mater. Chem.* **2001**, *11*, 2095−2101.

10.1021/ja0474244 CCC: $27.50

salts containing monomeric hallometalate FeX_4^- (X = Cl, Br) anions.[9,10] More recently Coronado et al.[11] reported on a ferromagnetic molecular metal of formula β-(BEDT-TTF)$_3$[MnCr(C_2O_4)$_3$] whose structure is closely related to the tris-oxalato-metalate (III) paramagnetic superconductors in which the A = H_3O^+ cation has been replaced by Mn(II). Chalcogenide rhenium clusters have also been used in association with TTF-based cation radical molecules to construct molecular architectures aimed to combine electronic and magnetic properties.[12] In all cases, these hybrid materials are formed by segregated networks of the two molecular components where the properties furnished by each network are quasi-independent due to the weakness of the electronic interactions between them. This feature is in sharp contrast with what is found in classical magnetic conductors such as iron or gadolinium in which magnetism and conductivity come from the same component and therefore cannot be decoupled.

Here we report the preparation of a new single-component molecular material that lies at the crossing of two research avenues: conductivity and magnetism. Single-component molecular conductors are usually based on mononuclear transition metal complexes with extended-TTF dithiolate ligands and recent efforts are being made to produce molecule-based conducting magnets using these dithiolate complexes with magnetic metals. The existence of conduction paths in these systems has been associated with the sulfur π-orbitals and with the formation of S−S networks with transversal contacts that result in 3-D materials. We have explored the possibility of replacing the transition metal in these mononuclear complexes by the trinuclear cluster unit formulated as [Mo_3(μ_3-S)(μ_2-S_2)$_3$]$^{4+}$, where the metal atoms define an equilateral triangle capped by one apical μ_3-sulfur atom and with the Mo atoms bridged by disulfide ligands that results in idealized C_{3v} symmetry for this cluster core. One remarkable feature of this Mo_3S_7 unit is the electrophilic character of the axial sulfur atoms (S_{ax}), those out of the Mo_3 plane, which provides this cluster core with a high potential as building block for the formation of supramolecular adducts.[13]

2. Results and Discussion

Derivatives with Mo_3S_7 units are readily accessible from the [$Mo_3S_7Br_6$]$^{2-}$ complex due to the lability of the bromine ligands.[14] This cluster unit is electron precise with six metal "d" electrons available to enter the low energy $1a_1$ and 1e metal cluster orbitals, which correspond to three metal−metal bonding orbitals and a formal oxidation state of +4 for the molybdenum atoms.[15,16] Although Mo_3S_7 compounds show waves in their cyclic voltagram assigned to the μ_2-S_2 reduction, most of these complexes do not present oxidation processes. However, substitution of the bromine atoms in [$Mo_3S_7Br_6$]$^{2-}$ by the organic dmit (1,3-dithia-2-thione-4,5-dithiolate) ligand gives the [Mo_3S_7(dmit)$_3$]$^{2-}$ ([**1**]$^{2-}$) anion, which shows a two-electron quasireversible wave at easily accessible potentials, 0.38 V vs E(ferrocenium/ferrocene). The shape of this wave on the reverse scan is indicative of the buildup of conductive species at the electrode. This facile oxidation upon ligand substitution results in a change from a $1a^22e^4$ to a $1a^22e^2$ ground-state configuration suggesting the presence of a significant contribution of the dithiolate ligand to the HOMO "e" orbital, which leads to a partial occupation of the degenerate HOMO orbitals with the concomitant production of radicals, a prerequisite in the formation of single component molecular conductors. In addition, this two-electron oxidized molecule is also interesting from the magnetic point of view since it should have a spin S = 1.

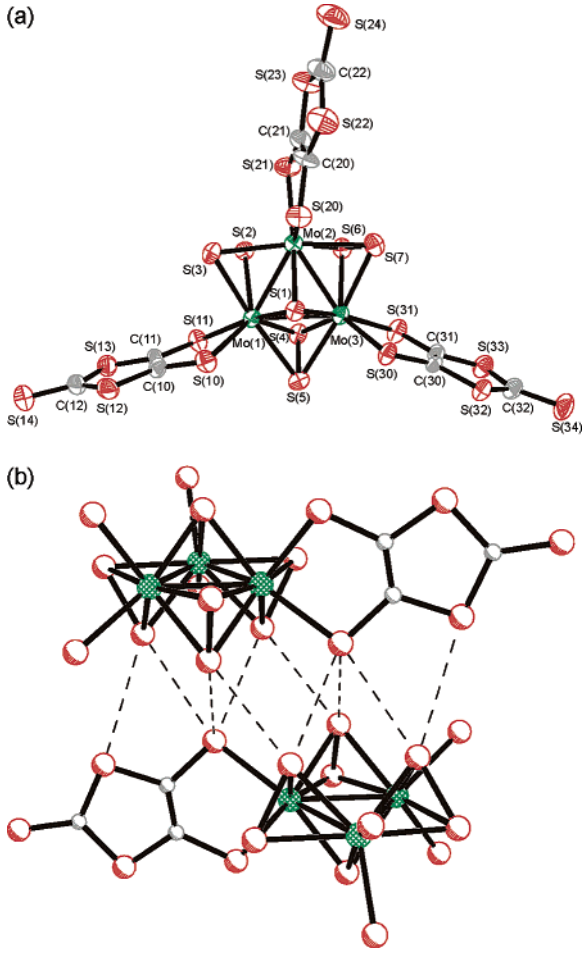

Figure 1. (a) ORTEP representation of the [Mo_3S_7(dmit)$_3$]$^{2-}$ anion (50% probability ellipsoids) with the atom numbering scheme (b) Dimer formation in the structure of [**1**]$^{2-}$.

The molecular structures of the tetrabuthylammonium and tetraphenylphosphonium salts of the anion [**1**]$^{2-}$ represented in Figure 1a, show the main structural features reported for other Mo_3S_7 derivatives with the outer dmit ligands oriented almost perpendicular to the trimetallic plane. In these structures the [Mo_3S_7(dmit)$_3$]$^{2-}$ anionic cluster reveals characteristic interactions between the axial (out of plane) sulfur atoms of the disulfide bridges and the sulfur atoms of the dmit ligand in the neighboring cluster that yield to dimer formation (Figure 1b). Such dimerization has already been observed in other dithiolate

(9) Kobayashi, H.; Tomita, H.; Naito, T.; Kobayashi, A.; Sakai, F.; Watanabe, T.; Cassoux, P. *J. Am. Chem. Soc.* **1996**, *118*, 368−377.
(10) Ojima, E.; Fujiwara, H.; Kato, K.; Kobayashi, H.; Tanaka, H.; Kobayashi, A.; Tokumoto, M.; Cassoux, P. *J. Am. Chem. Soc.* **1999**, *121*, 5581−5582.
(11) Coronado, E.; Galán-Mascarós, J. R.; Gómez-García, C.; Laukhin, V. *Nature* **2000**, *408*, 447−449.
(12) Gabriel, J. C. P.; Boubekeur, K.; Uriel, S.; Batail, P. *Chem. Rev.* **2001**, *101*, 2037−2066.
(13) Garriga, J. M.; Llusar, R.; Uriel, S.; Vicent, V.; Usher, A. J.; Lucas, N. T.; Humphrey, M. G.; Samoc, M. *J. Chem. Soc., Dalton Trans.* **2003**, 4546−4551.
(14) Fedin, V. P.; Sokolov, M. N.; Fedorov, V. Y.; Yufit, D. S.; Struchkov, Y. T. *Inorg. Chim. Acta* **1991**, *179*, 35−40.
(15) Müller, A.; Jostes, R.; Cotton, F. A. *Angew. Chem., Int. Ed. Engl.* **1980**, *19*, 875−882.
(16) Mayor-López, M. J.; Weber, J.; Hegetschweiler, K.; Meienberger, M. D.; Joho, F.; Leoni, S.; Nesper, R.; Reiss, G. J.; Frank, W.; Kolesov, B. A.; Fedin, V. P.; Fedorov, V. E. *Inorg. Chem.* **1998**, *37*, 2633−2644.

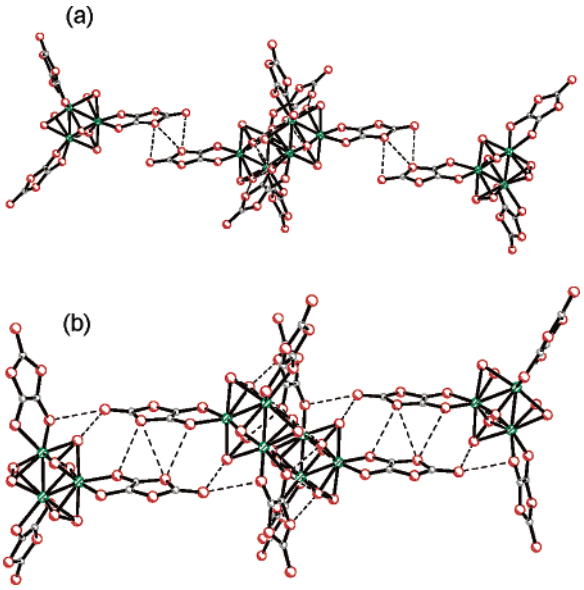

Figure 2. Packing diagram for compounds $((n\text{-}Bu)_4N)_2$[**1**] (a) and $(PPh_4)_2$-[**1**] (b), showing the cluster dimers and the S···S interactions between dimers. Mo atoms in green and sulfur atoms in red.

Mo_3S_7 complexes.[13] Additional interactions between one of the dmit ligands that does not participate in the dimer formation with the inversion-center-symmetry-related dmit on a neighbor cluster gives rise to the formation of infinite chains along the [101] and *b* directions for complexes $((n\text{-}Bu)_4N)_2$[1] and $(PPh_4)_2$-[1], respectively. The nature of these interactions depends on the counterion, which is again a sign of the structural versatility of these cluster units. In the case of complex $((n\text{-}Bu)_4N)_2$[**1**] the chain formation involves the outer sulfur atoms of the dmit ligand with contacts that range between 3.213 and 3.447 Å (Figure 2 a). In the structure of $(PPh_4)_2$[**1**] the outer sulfur atom interacts with the cluster core sulfur atom, together with lateral contacts between the dmit ligands, through the remaining sulfur atoms (Figure 2b). The differences in crystal packing are also reflected in the orientation of the dithiolate ligands with regard to the metal atoms' plane. In the structures $((n\text{-}Bu)_4N)_2$[**1**] and $(PPh_4)_2$[**1**], the plane that contains the dmit ligand involved in the dimer formation is folded along the S−S hinge by 18.4° and 10.3°, respectively while folding angles of 12.2° for $((n\text{-}Bu)_4N)_2$[**1**] and 7.3° for $(PPh_4)_2$[**1**] are observed for the ligand that participates in the chain formation. The third dmit ligand, with no intermolecular interactions, shows the lower folding angles, 7.2 and 1.5° for $((n\text{-}Bu)_4N)_2$[**1**] and $(PPh_4)_2$[**1**] respectively.

Electrochemical oxidation of acetonitrile solutions containing $((n\text{-}Bu)_4N)_2[Mo_3S_7(dmit)_3]$ with an excess of $((n\text{-}Bu)_4N)Br$ gives dark violet air-stable needle crystals of composition $Mo_3S_7(dmit)_3$ (**1**). This complex can alternatively be synthesized as a black microcrystalline powder by chemical oxidation of $((n\text{-}Bu)_4N)_2[Mo_3S_7(dmit)_3]$ in dichloromethane with iodine in an almost quantitative yield. Neutral $Mo_3S_7(dmit)_3$ molecules crystallize in a hexagonal space group with the cluster units oriented along the *c* direction through S···S interactions of 3.6 Å between the electrophilic axial sulfur atoms of one cluster and the capping sulfur atom of the adjacent cluster to produce infinite chains as depicted in Figure 3a with additional S···S contacts between the dithiolate sulfur atoms on contiguous clusters. The distance between metal planes is ca. 6.5 Å. Parallel

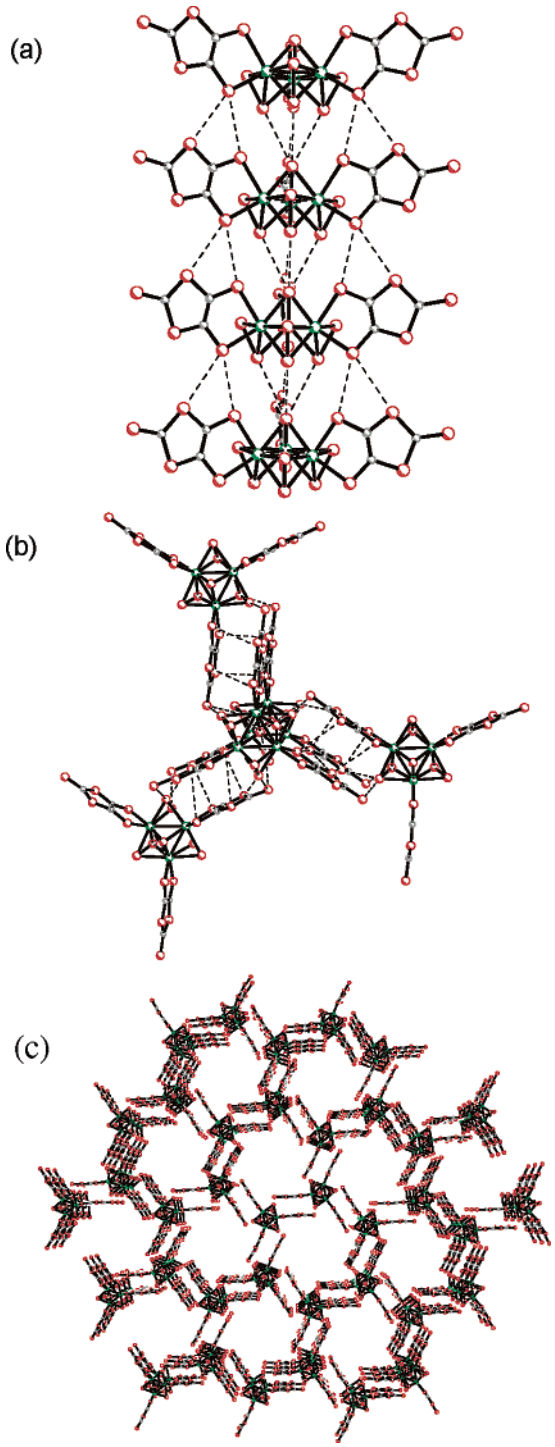

Figure 3. Crystal structure of $Mo_3S_7(dmit)_3$: (a) Packing of the $Mo_3S_7(dmit)_3$ units along the *c* direction and (b) along the *ab* plane with intermolecular S···S interactions shown as dashed lines; (c) a view in the *c* direction of the resulting honeycomb arrangement showing the cavities distribution. Mo atoms in green and sulfur atoms in red.

chains are related by an inversion center and connected through short contacts (3.1 to 3.5 Å) across the *ab* plane between the dmit sulfur atoms of one cluster chain and the bridging cluster sulfur atoms on the next chain and longer S···S contacts (3.7 to 4.0 Å) between dmit ligands as shown in Figure 3b. This packing results in an extended hexagonal network represented in Figure 3c with threefold symmetry molecular units and partially filled molecular orbitals. In addition, the resulting structure contains large open channels of ca. 10 Å in diameter.

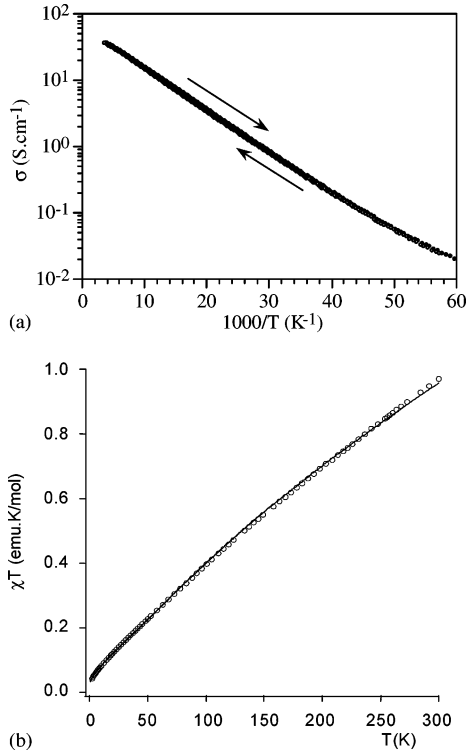

Figure 4. Transport and magnetic properties of $Mo_3S_7(dmit)_3$: (a) Temperature dependence of the conductivity for a single-crystal sample; (b) χmT versus T representation for a polycrystalline sample. The solid line is reproduced using the theoretical model described in text.

Changes that are not statistically significant are found for the Mo−Mo, Mo−$S_{cluster}$, and Mo−S_{dmit} bond distances upon oxidation. In the same manner, the dmit C═C bond remains unaffected in going from $[Mo_3S_7(dmit)_3]^{2-}$ to $Mo_3S_7(dmit)_3$, in contrast with the observations reported for the $[M(dmit)_2]^{n-/0}$ system where the Raman frequency of the C═C stretching mode increases with the formal charge.[17]

The dc electrical conductivities were measured on compacted pellets and single-crystal samples. The room-temperature conductivities, σ(RT), along the c axis of nine different needle-shape single crystals vary between 5 and 50 S/cm with an average value of 25 S/cm. The neutral $Mo_3S_7(dmit)_3$ is a semiconductor (Figure 4a) with a small activation energy of 12−22 meV. Pressed pellets of powder samples gave σ(RT) = 1−2 S cm^{-1} with activation energies of 33−35 meV. Dai et al.[18] have previously shown that partial oxidation of a tetranuclear Cu(I) cluster dianion coordinated to a TTF-derived dithiolate produces a semiconducting material with σ(RT) = 3.5×10^{-4} S cm^{-1}, although no characterization of the oxidized product is reported. Conductivity measurements of two single crystals of **1** under pressure show an increase in the room-temperature conductivity at a rate of 1−5 S cm^{-1} $kbar^{-1}$ and a decrease of the activation energy with applied pressure at a rate of 0.05−0.17 meV $kbar^{-1}$, although no metallic behavior was observed below 10 kbar. These results indicate that the compound is semiconductor with a very low activation energy. The increase in the conductivity values and the decrease in the energy gap with applied pressure may be attributed to a shortening of the intermolecular distances along the needle axis (c-axis).

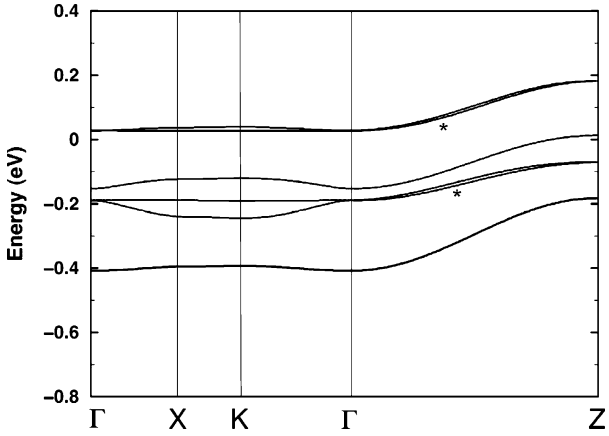

Figure 5. AFM band structure of $Mo_3S_7(dmit)_3$ (**1**) where Γ: (0, 0, 0), X: (1/2, 0, 0), K: (1/3, 1/3, 0), and Z: (0, 0, 1/2) in units of the reciprocal lattice vectors.

The magnetic susceptibility, measured on a polycrystalline sample, shows a continuous decrease in the χT vs T plot upon cooling (Figure 4b). At room temperature the χT value equals 0.80 emu K mol^{-1}, which is clearly below the value expected for a spin triplet (1 emu K mol^{-1}). This low room-temperature value, together with the significant decrease in χT, indicate the presence of antiferromagnetic exchange interactions between the unpaired electrons of the neutral $Mo_3S_7(dmit)_3$ molecules. To undertake a quantitative analysis of these magnetic data we have first investigated the electronic structure of this molecular solid. Theoretical calculations using first-principles spin-polarized DFT type calculations for both the ferromagnetic (FM) and antiferromagnetic (AFM) states revealed that both states are very close in energy with the AFM state lying 0.02 eV/molecule below the FM state, something that is consistent with the susceptibility measurements.

The calculated band structure for the AFM state is shown in Figure 5 where every band is really the superposition of two bands, one with alpha spin and one with beta spin. Our calculations for both the isolated molecule and the solid lead to a clear-cut view of this AFM state. Because of the threefold symmetry, the highest occupied levels of the isolated molecule are a set of degenerate orbitals (e-type) that contains two electrons. In agreement with Hund's rule, the more stable situation corresponds to a triplet coupling between the two electrons. Going from the isolated molecule to the solid, stabilizing intermolecular interactions along the c-direction develop. That is, there is an antiferromagnetic coupling between adjacent triplet states, leading to an AFM state. The bands in Figure 5 originating from these e-type levels (notice that there are two molecules per repeat unit) are marked with an asterisk. The remaining bands originate from the nondegenerate a-type counterpart of these e-type levels. Since there are four electrons per molecule to fill these bands, the two pairs of a-type bands and the two lower pairs of e-type bands are filled so that a very small gap separates the top of the highest filled and lowest empty bands. As shown in Figure 5 the bands show dispersion along the c*-direction (i.e., Γ → Z) but are considerably flatter in the (a*b*)-plane (see the Γ → X → K → Γ directions). This clearly shows the existence of predominant electronic interactions along the c-direction for the electrons near the Fermi level so that

(17) Cassoux, P. *Coord. Chem. Rev.* **1999**, *186*, 213−232.
(18) Dai, J.; Munakata, M.; Ohno, Y.; Bian, G. Q.; Suenaga, Y. *Inorg. Chim. Acta* **1999**, *285*, 332−335.

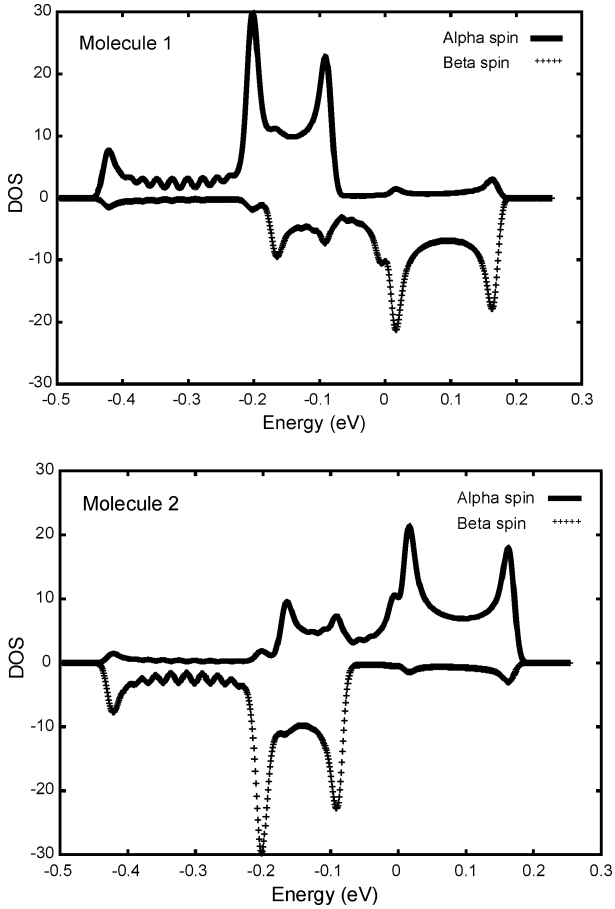

Figure 6. Projected density of states of complex **1** associated with the two different molecules of the unit cell.

$Mo_3S_7(dmit)_3$ is a new pseudo-one-dimensional magnetic semiconductor. The important observation from the band structure is that in addition to the non negligible dispersion along *c*, there is an extremely small energy gap at the Fermi level, something that harmonizes with the activated although high conductivity of the system.

To substantiate the description above we show in Figure 6 the partial Density of States (PDOS) associated with the two different molecules of the unit cell (note that the small energy gap separating the filled and empty bands is not visible in these curves because of the smoothing used to generate the PDOS). Looking, for instance, at the PDOS of Figure 6 (i.e., the contribution of molecule 1), the more prominent feature is the double-peaked alpha spin contribution centered around −0.13 eV. This is the typical shape of a DOS contribution associated with a pseudo-one-dimensional band. Comparing Figures 5 and 6 it is clear that this contribution originates from the filled double pair of e-type bands. A beta spin contribution appears in the same energy region associated with the upper pair of a-type bands; lower in energy there is an alpha spin contribution arising from the lower pair of a-type bands. The beta spin counterpart of the double-peaked contribution appears in the empty states region. The same description applies to molecule 2 except that the filled part of the e-type levels corresponds now to the beta spin states and the empty one to the alpha spin states. Consequently, every molecule contributes with one alpha spin and one beta spin electron in a-type levels whereas molecule 1 contributes with two alpha spin electrons and molecule 2 with two beta spin electrons in e-type levels. This is the signature of an AFM state.

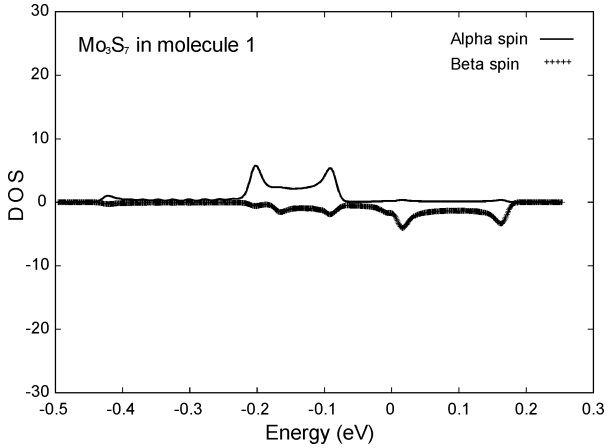

Figure 7. Projected density of states of complex **1** associated with the inner Mo_3S_7 cluster unit of molecule 1.

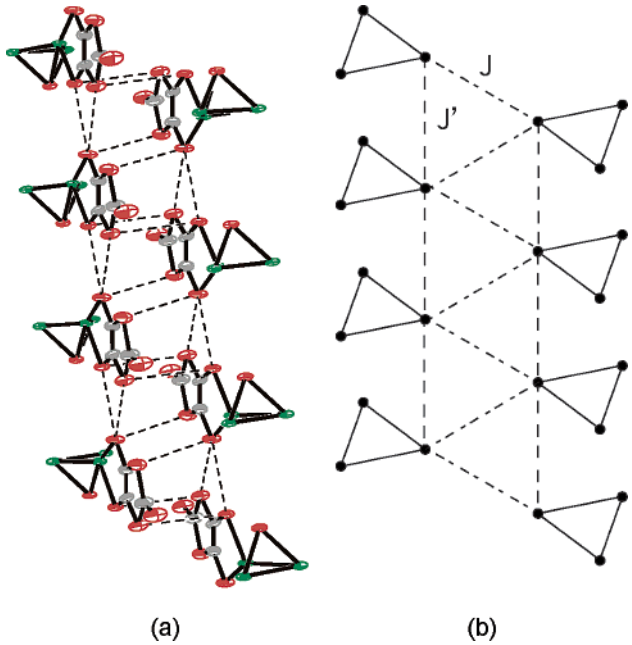

Figure 8. (a) Partial representation of the $Mo_3S_7(dmit)_3$ structure along the *c* axis emphasizing the S···S interactions responsible for the conduction paths. Only two adjacent cluster chains and one dmit ligand per cluster are represented. Bridging disulfides within the cluster core have been omitted for clarity (b) Exchange network of the $Mo_3S_7(dmit)_3$ structure showing the two different exchange parameters J and J′.

It is important to understand the origin of the band dispersion along *c*. Shown in Figure 7 is the contribution of the inner Mo_3S_7 cluster unit to the PDOS of Figure 6. This contribution is nonnegligible but only between 1/4 and 1/6 of the total. Although not shown here, exactly the same result applies for molecule 2. Thus, the dmit contributions dominate in this energy region as suggested by the chemical results. Consequently, the short intermolecular contacts associated with the atoms of the inner cluster unit will not effectively contribute to the band dispersion. The energy dispersion along the *c**-direction is mainly due to short S···S contacts between dmit units of different clusters. As shown in Figure 8a there are two types of contacts of this kind: those between translationally equivalent (i) and those between non translationally equivalent (ii) dmit units. Although the first ones are shorter (between 3.4 and 3.8

Å), the orbital interactions are mostly π-type and are consequently weak. The dispersion is mainly due to the two pairs of S···S (3.713(x2) Å and 3.966(x2) Å) contacts of the second type in which every dmit is implicated. As shown in Figure 8, a zigzag chain of these contacts develops along the *c*-direction. Since these dmit units are locally almost parallel the orbital orientation leads to a quite favorable interaction and thus, to the band dispersion along the *c**-direction. Although not shown in Figure 8, there is also one pair of C···S contacts (3.714(x2) Å that, because of excellent orbital interaction, have also a non negligible contribution. Let us note that because of the very delocalized nature of the a- and e-type molecular levels leading to the bands in Figure 5, the intrasite repulsion energies (*U*) must be considerably lower than in the molecules usually employed for the synthesis of molecular conductors. For instance, whereas values of approximately 1 eV have been suggested for Ni(dmit)$_2$,[19] our calculations suggest values approximately four times smaller for $Mo_3S_7(dmit)_3$. This means that quite modest energy dispersions could lead to a metallic behavior for systems such as those discussed here. In fact, the hypothetical metallic state for $Mo_3S_7(dmit)_3$ solid was calculated to be only 0.05 eV/molecule higher in energy that the AFM state. Chemical modifications combined with pressure application would be extremely interesting to see if the metallic state could be stabilized.

Let us now return to the modeling of the magnetic properties. In view of the electronic interactions pointed out by the above calculations we have decided to take into account the interactions along the *c* direction as described in Figure 8a. This gives rise to a magnetic lattice formed by magnetic chains of $Mo_3S_7(dmit)_3$ clusters along the *c* direction that are coupled through the dmits within and between chains to give rise to a three-dimensional exchange network. If only two adjacent chains of clusters are considered, the magnetic lattice reduces to a one-dimensional exchange network formed by $S = 1$ magnetic clusters with nearest-neighbor and next-nearest-neighbor interactions (Figure 8b). The nearest-neighbor interaction, *J*, corresponds to the exchange pathway through dmit ligands belonging to different chains, and the next-nearest-neighbor interaction, *J*′, to the exchange pathway through dmits belonging to the same chain of clusters. Each magnetic cluster is in fact a mixed-valence system containing two unpaired electrons delocalized over three sites. Therefore, the magnetic model should also take into account the electron-transfer processes occurring inside the $S = 1$ cluster. A convenient way to do so is to consider a localized spin chain formed by a random distribution of spins $S = 0$ or $S = 1$ over each interacting site, with probabilities 1/3 and 2/3, respectively. Such a model accounts for the possible distributions of the two electrons inside the mixed-valence cluster. Thus, when the dmit site involved in the exchange network contains one electron, the local spin of the cluster is 1, as it can interact with the spins of the neighboring clusters, while when this dmit site contains the hole, the local spin is 0 as the exchange interactions along the chain are interrupted. As one can see in Figure 4b this kind of model closely reproduces the experiment in the whole temperature range. The resulting parameters are $J = -66$ cm^{-1}, $J' = -13.2$ cm^{-1}, $g = 1.92$, and TIP $= 2 \times 10^{-3}$ emu/mol (solid line in Figure 4b). Notice that the g-value is within the values reported for similar molybdenum clusters.[20] On the other hand, a non-negligible temperature-independent paramagnetism (TIP) has been considered to fit the high-temperature region. This contribution probably comes from the Pauli paramagnetism of the conducting system, although the molybdenum cluster may also contribute to this term. From these results the magnetic lattice of this molecular conductor may be viewed as formed by random fragments of exchange-coupled mixed-valence $Mo_3S_7(dmit)_3$ clusters wherein two antiferromagnetic interactions compete to give rise to a spin frustrated extended network. This frustration is probably at the origin of the lack of long magnetic order in the material.

3. Experimental Section

3.1 General. All reactions were performed under a positive pressure of nitrogen. Compounds $(NH_4)_2[Mo_3S_{13}]$[21] and $((n\text{-}Bu)_4N)_2(Zn(dmit)_2$[22] were prepared according to the literature. The compound $((n\text{-}Bu)_4N)_2[Mo_3S_7Br_6]$ was prepared as previously described but using the tetrabutylammonium salt of the trinuclear starting materials instead of tetraethylammonium.[23] Elemental analyses were carried out with a C. E. analyzer, model EA 1108. IR spectra were recorded on a Perkin-Elmer System 2000 FT-IR using KBr pellets. Raman spectra were recorded on a Perkin-Elmer System 2000 NIR−FT. The vibrational bands assignments reported below are based on previously reported data for related complexes.[24,25] Raman spectrum for complex $Mo_3(\mu_3\text{-}S)(\mu_2\text{-}S_2)_3(dmit)_3$ (**1**) consists of very broad signals centered around 1000 and 700 cm^{-1} being a sign of the sample overheating or burning up, thus precluding a reliable comparison between the Raman spectra of the dianionic $[\mathbf{1}]^{2-}$ and neutral **1** complexes. Electrospray mass spectra were recorded with a Micromass Quattro LC instrument. Cyclic voltammetry experiments on $((n\text{-}Bu)_4N)_2[Mo_3S_7(dmit)_3]$ were performed in CH_2Cl_2 with an Echochemie Pgstat 20 electrochemical analyzer and a conventional three-electrode configuration consisting of platinum working and auxiliary electrodes and a Ag/AgCl reference electrode.

(a) Preparation of $((n\text{-}Bu)_4N)_2[Mo_3(\mu_3\text{-}S)(\mu_2\text{-}S_2)_3(dmit)_3]$ ($((n\text{-}Bu)_4N)_2$ [1]). An orange solution of $((n\text{-}Bu)_4N)_2[Mo_3S_7Br_6]$ (200 mg 0.17 mmol) in acetonitrile (60 mL) was reacted with $((n\text{-}Bu)_4N)_2$ ($Zn(dmit)_2$) (300 mg, 0.318 mmol) and the mixture was refluxed for 4 h. The dark-red solution was taken to dryness under vacuum and the dark-red precipitated was washed with methanol to eliminate excess of $((n\text{-}Bu)_4N)_2(Zn(dmit)_2)$ and diethyl ether. The residue was recrystallized from CH_2Cl_2/ether to give violet cubic crystals suitable for X-ray analysis characterized as $(((n\text{-}Bu)_4N)_2$ [**1**]). (161 mg, 60%). Anal. Calcd. for $Mo_3S_{22}C_{41}H_{72}N_2$: C, 31.04; H 4.58, N, 1.77, S, 44.47. Found: C, 31.12; H, 4.50; N, 0.98; S, 45.24. IR cm^{-1}: 2955(s), 2885 (m), 1455 (C═C, s), 1050 (C═S, vs), 1025 (C═S, s), 557 (S_e-S_a, m), 510 (m), 466 (m); Raman (350mW) cm^{-1}: 1453 (C═C, s), 1050 (C═S, w), 561 (S_e-S_a, w), 515 (w), 466 (m), 379 (w), 354 (w), 305 (w), 285 (w), 253 (w), 183 (Mo−Mo, m). Electrospray-MS (cone = 20V, CH_2Cl_2); *m*/*z* 551 $[Mo_3S_7(dmit)_3]^{2-}$, 1344 $[(n\text{-}Bu)_4NMo_3S_7(dmit)_3]^-$.

(b) Preparation of $Mo_3(\mu_3\text{-}S)(\mu_2\text{-}S_2)_3(dmit)_3$ (1). Chemical oxidation of dichloromethane solutions of $((n\text{-}Bu)_4N)_2[Mo_3S_7(dmit)_3]$ (200 mg, 0.13 mmol) with an excess of I_2 (5 mL of a 0.1 M acetonitrile solution, 0.5 mmol) causes immediate precipitation of a violet solid. The solid was separated by filtration and characterized as **1**

(19) Doublet, M.-L.; Lepetit, M.-B. *J. Chem. Phys.* **1999**, *110*, 1767−1773.
(20) Miyamoto, R.; Kawata, S.; Iwaizumi, M.; Akashi, H.; Shibahara, T. *Inorg. Chem.* **1997**, *36*, 542−546.
(21) Müller, A.; Sarkar, S.; Bhattacharyya, R. G.; Pohl, S.; Dartmann, M. *Angew. Chem., Int. Ed. Engl.* **1978**, *17*, 535−539.
(22) Steimecke, G.; Sieler, H. J.; Kirmse, R.; Hoyer, E. *Phosphorus Sulfur* **1979**, *7*, 49−55.
(23) Fedin, V. P.; Mironov, Y. V.; Sokolov, M. N.; Kolesov, B. A.; Fedorov, V. Y.; Yufit, D. S.; Struchkov, Y. T. *Inorg. Chim. Acta* **1990**, *174*, 275−282.
(24) Pokhodnya, K. I.; Faulmann, C.; Malfrant, I.; Andreu-Solano, R.; Cassoux, P.; Mlayah, A.; Smirnov, D.; Leotin, J. *Synth. Met.* **1999**, *103*, 2016−2019.
(25) Liu, G.; Fang, Q.; Xu, W.; Chen, H.; Wang, C. *Spectrochim. Acta, Part A* **2004**, *60*, 541−550.

Table 1. Crystallographic Data for $((n\text{-Bu})_4N)_2[Mo_3(\mu_3\text{-S})(\mu_2\text{-S}_2)_3(dmit)_3]$ ($(n\text{-Bu})_4N)_2$[**1**]), $(PPh_4)_2[Mo_3(\mu_3\text{-S})(\mu_2\text{-S}_2)_3(dmit)_3]$ ($(PPh_4)_2$[**1**]), and $Mo_3(\mu_3\text{-S})(\mu_2\text{-S}_2)_3(dmit)_3$ (**1**)

	$((n\text{-Bu})_4N)_2$ [**1**]	$(PPh_4)_2$[**1**]	(**1**)
formula	$C_{41.50}H_{73}ClMo_3N_2S_{22}$	$C_{57}H_{40}Mo_3P_2S_{22}$	$C_9Mo_3S_{22}$
formula wt	1628.61	1779.97	1101.23
crystal system	monoclinic	triclinic	trigonal
a, Å	16.135(6)	15.784(4)	19.439(3)
b, Å	24.632(8)	16.137(4)	19.439(3)
c, Å	17.983(7)	16.380(4)	6.5573(19)
α, deg		64.733(7)	
β, deg	109.177(7)	70.887(7)	
γ, deg		76.725(7)°	
V, Å^3	6751(4)	3545.2(16)	2145.8(8)
T, K	233(2)	293(2)	233(2)
space group	P2(1)/n	P-1	P-3
Z	4	2	2
μ, mm^{-1}	1.300	1.253	1.939
θ range, deg	1.46−23.25	1.37-23.25	1.21−24.65
refl. collected	31 847	17 418	11 950
unique refl/R_{int}	9404/0.1352	10 172/0.0690	2441/0.0862
$R1^a/wR2^b(I>2\sigma)$	0.0625/0.1322	0.0641/0.1555	0.0824/0.2412
GOF	1.024	1.030	1.092

[a] $R1 = \sum||F_o| - |F_c||/\sum F_o$. [b] $wR2 = [\sum[w(F_o^2 - F_c^2)^2]/\sum[w(F_o^2)^2]]^{1/2}$.

(130 mg, 94%). Single-crystal growth was carried out electrochemically in a conventional H-shaped cell. Acetonitrile solutions of $((n\text{-Bu})_4N)_2[Mo_3S_7(dmit)_3]$ (15 mg) and TBABr (25 mg) were placed in both compartments and a constant current of 0.4 μA was applied for 21 days at room temperature to give dark-violet air-stable needle crystals suitable for diffraction studies of complex **1**.

Anal. Calcd. for $Mo_3S_{22}C_9$: C, 9.82; S, 64.05. Found: C, 10.12; S, 65.24. IR cm^{-1}: 1200 (C═C, m broad), 1047 (C═S, vs), 1016 (C═S, s), 507 (S_e-S_a, m), 472 (m), 437 (m).

3.2 Structural Studies. Crystals for X-ray studies of the tetraphenylphosphonium salt of [**1**]$^{2-}$ were obtained by addition of an excess of $(PPh_4)Br$ to a CH_2Cl_2 solution of $((n\text{-Bu})_4N)_2$[**1**] and further recrystallization from CH_2Cl_2/ether.

Single crystals of $((n\text{-Bu})_4N)_2$[**1**] and (**1**) were mounted on a glass fiber with silicon grease and transferred to a nitrogen flow at −40 °C. A crystal of $(PPh_4)_2$[**1**] was mounted on the tip of a glass fiber with the use of epoxy cement and measured at 25 °C. X-ray diffraction experiments were carried out on a Bruker SMART CCD diffractometer using Mo−Kα radiation (λ = 0.71 073 Å). The data were collected with a frame width of 0.3° in Ω at a crystal to detector distance of 4 cm. The software SAINT[26] was used for integration of intensity reflections and scaling and the software SADABS[27] was used for absorption correction. Final cell parameters were obtained by global refinement of reflections obtained from integration of all the frames data. The crystal parameters and basic information relating data collection and structure refinement for compounds $((n\text{-Bu})_4N)_2$[**1**], $(PPh_4)_2$[**1**] and (**1**) are summarized in Table 1.

The structures were solved by direct methods and refined by the full-matrix method based on F using the SHELXTL software package.[28] The nonhydrogen atoms of the cluster in structures $((n\text{-Bu})_4N)_2$[**1**], $(PPh_4)_2$[**1**], and (**1**) were refined anisotropically; the positions of all hydrogen atoms of tetrabutylammonium and tetraphenylphosphonium cations in structures $((n\text{-Bu})_4N)_2$[**1**] and $(PPh_4)_2$[**1**] were generated geometrically, assigned isotropic thermal parameters, and allowed to ride on their respective parent carbon atoms. The last difference Fourier map in structure $((n\text{-Bu})_4N)_2$[**1**] showed the presence of a molecule of CH_2Cl_2 that was refined with 1/2 partial occupancy.

3.3 Magnetic Measurements and Modeling. Magnetic measurements were done on a polycrystalline sample with a commercial SQUID susceptometer (Quantum Design MPMS-XL-5) in the temperature range 2−300 K with an applied magnetic field of 0.05 T. The sample susceptibility was corrected for the sample holder contribution, previously measured in the same conditions, and for the diamagnetic contribution of the constituent atoms (Pascal's tables). A computational procedure based on closed-chain calculations has allowed us to evaluate the magnetic properties of the different spin distributions.[29] In the present case the size of the matrices to be diagonalized and the computing times have limited the calculations to 12 sites, which is good enough to reproduce the behavior of the infinite chain in the temperature range of interest. By adding up the curves of the different spin distributions, taking into account the probability of each distribution to occur, one can finally obtain the behavior of the system for different values of the ratio J'/J.

3.4 Conductivity Measurements. The dc conductivity measurements over the range 2−300 K were performed with the standard two-contacts method on nine different single crystals (needles of typical dimensions 0.2 × 0.02 × 0.02 mm^3) and with the four-contacts method on two pressed pellets with commercial equipment (Quantum Design PPMS-9). Contacts to the samples in all cases were made by platinum wires (25 μm diameter) attached by graphite paste to the samples. The cooling and warming rate was 1 K/min and the intensity of the applied dc current was 1 μA. Conductivity measurements under pressure were done with a homemade pressure cell. Hydrostatic pressure up to 10 kbar was applied using silicone oil. The pressure inside the cell was monitored measuring the resistivity of a previously calibrated manganin wire. The measurements under pressure were done at cooling and warming rates of 0.5 K/min with applied dc currents of 0.1 μA.

3.5 Computational Details. The first-principles spin-polarized calculations were carried out using a numerical atomic-orbitals DFT approach, which has been recently developed and designed for efficient calculations in large systems and implemented in the SIESTA code.[30] We have used the generalized gradient approximation to DFT and, in particular, the functional of Perdew et al.[31] Only the valence electrons are considered in the calculation, with the core being replaced by norm-conserving scalar relativistic pseudopotentials[32] factorized in the Kleinman-Bylander form.[33] We have used a split-valence double-ζ basis set including polarization orbitals for all atoms, as obtained with an energy shift of 10 meV.[34] A specially optimized basis set based on recent soft-potential techniques[35] has been used for Mo. The integrals of the self-consistent terms of the Kohn−Sham Hamiltonian are obtained with the help of a regular real-space grid in which the electron density is projected. The grid spacing is determined by the maximum kinetic energy of the plane waves that can be represented in that grid. In the present work, we used a cutoff of 135 Ry. The Brillouin zone was sampled using grids of (1 × 1 × 3) and (1 × 1 × 30) *k*-points[36] for total energy and projected density of states computations, respectively.

Acknowledgment. This work has been developed in the framework of a COST Action on Inorganic Molecular Conductors. Financial support by the "Ministerio de Ciencia y Tecnologia" (research projects BQ2002-00313, BFM2003-03372-C03 and MAT2001-3507), Generalitat de Catalunya (Project 2001

(26) *SAINT*; 5.0 ed.; Bruker Analytical X-ray Systems: Madison, WI, 1996.
(27) Sheldrick, G. M. *SADABS empirical absorption program*; University of Göttingen, 1996.
(28) Sheldrick, G. M. *SHELXTL*; 5.1 ed.; Brucker Analytical X-ray Systems: Madison, WI, 1997.
(29) Borrás-Almenar, J. J.; Clemente-Juan, J. M.; Coronado, E.; Tsukerblat, B. S. *Inorg. Chem.* **1999**, *38*, 6081−6088.
(30) Soler, J. M.; Artacho, E.; Gale, J. D.; Garcia, A.; Junquera, J.; Ordejon, P.; Sanchez-Portal, D. *J. Phys.: Condens. Matter* **2002**, *14*, 2745−2779.
(31) Perdew, J. P.; Burke, K.; Ernzerhof, M. *Phys. Rev. Lett.* **1996**, *77*, 3865−3868.
(32) Troullier, N.; Martins, J. L. *Phys. Rev. B* **1991**, *43*, 1993−2006.
(33) Kleinman, L.; Bylander, D. M. *Phys. Rev. Lett.* **1982**, *48*, 1425−1428.
(34) Artacho, E.; Sanchez-Portal, D.; Ordejon, D.; Garcia, A.; Soler, J. M. *Phys. Status Solidi B* **1999**, *215*, 809−817.
(35) Anglada, E.; Soler, J. M.; Junquera, J.; Artacho, E. *Phys. Rev. B* **2002**, *66*, 205101.
(36) Monkhorst, H. J.; Pack, J. D. *Phys. Rev. B* **1976**, *13*, 5188−5192.

SGR 333) and Fundació Caixa Castelló-UJI (research project P1.1B2001-07) is acknowledged. B. B. acknowledges support from the "Ministerio de Educación, Cultura y Deporte" of Spain. The computations were carried out using the resources of CESCA and CEPBA.

Supporting Information Available: X-ray crystallographic data, in CIF format. This material is available free of charge via the Internet at http://pubs.acs.org. Crystallographic data for the structural analyses have also been deposited with the Cambridge Crystallographic Data Centre, CCDC No. 222047 for $((n\text{-}Bu)_4N)_2[Mo_3S_7(dmit)_3]$ ($((n\text{-}Bu)_4N)_2$[**1**]), CCDC No. 237072 for $(Ph_4P)_2[Mo_3S_7(dmit)_3]$ ($(Ph_4P)_2$[**1**]), and CCDC No. 222048 for $Mo_3S_7(dmit)_3$ (**1**). Copies of this information may be obtained free of charge from The Director, CCDC, 12 Union Road, Cambridge CB2 1EZ, United Kingdom (fax /44-1223-336-033; e-mail deposit@ccdc.cam.ac.uk or http://www.ccdc-.cam.ac.uk). Structure factors are available on request from the authors.

JA0474244